

# A Rational Design of Catechol-Based Compounds: An Experimental and Theoretical Study of Optical Properties

Christophe Aronica,<sup>[a]</sup> Anna Venancio-Marques,<sup>[a]</sup> Jérôme Chauvin,<sup>[b]</sup>  
Vincent Robert,<sup>\*[a]</sup> and Gilles Lemerrier<sup>\*[a, c]</sup>

**Abstract:** The synthesis and optical properties of 4,5-disubstituted (*tert*-butyldimethylsilyloxy)-protected catechol derivatives are reported. One or two carbon–carbon triple bond functions were introduced through the Sonogashira cross-coupling reaction. The effects on the optical properties of mono-substitution at the 4-position or disubstitution at the 4- and 5-positions of

these catechol derivatives with electron-withdrawing or -donating substituents have been investigated. The experimental chemical-structure–polarisability

**Keywords:** charge transfer • density functional calculations • luminescence • nonlinear optics • polarizability

relationship has been studied by using the Lippert–Mataga correlation and compared with the results of a theoretical study carried out with DFT calculations. These compounds are promising candidates for the fine-tuning of internal charge transfer, but also as potential non-linear chromophores and ligands within multifunctional coordination complexes.

## Introduction

The prevalence of intramolecular charge-transfer (ICT) in organic molecules and related polymers<sup>[1]</sup> have motivated a large number of studies in the field of optoelectronics, for example, in electroluminescence devices (LEDs), thin-film transistors, solar cells and optical storage devices.<sup>[2]</sup> These compounds are commonly based on conjugated electron-withdrawing and -donating groups linked through a  $\pi$ -conjugated system. To target specific properties and applications, knowledge of a material's structure–property relationship

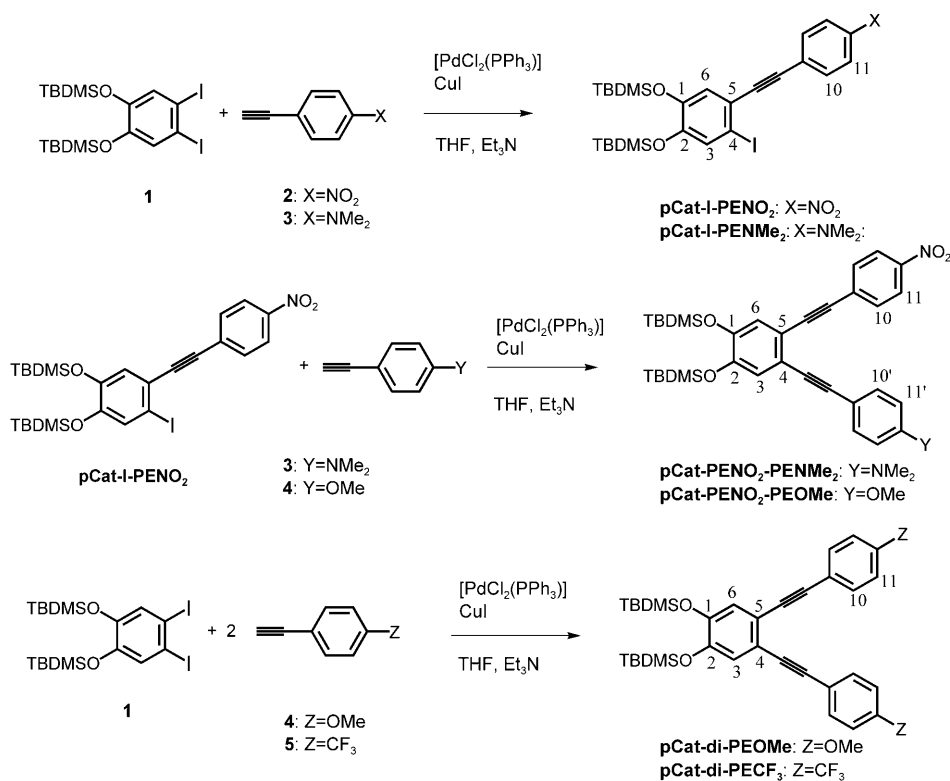
would be desirable. With this goal in mind, one may wonder how much the natures and positions of different groups control the optical properties and more particularly the polarisabilities of a material. Part of the answer is to be found in the modulation of the electron-transfer processes, which involve the donor (D) and acceptor (A) partners. As shown, for example, with substituted tetraethynylethenes,<sup>[3]</sup> the optical properties can be selectively varied by varying the substitution pattern and the nature of the substituents around the  $\pi$ -conjugated system. Thus, starting from a catecholate backbone, we contemplated the substitution of the 3- to 6-positions (see Scheme 1) with a view to generating disubstituted derivatives that could then be used for further complexation to a metal centre. Because our goal was to enhance the polarisabilities of a molecule for non-linear optical (NLO) applications, the design of molecules with large intramolecular charge transfer through chemical engineering is favoured. This can be achieved by concentrating on the 4- and 5-positions (see Scheme 1). At this stage, (D,D), (D,A) and (A,A) pairs of substituents were considered as promising candidates. Indeed, the (D,D) and (A,A) combinations should allow for charge transfer (CT) between the catecholate positions and the substituents. On the other hand, (D,A) substituents are likely to favour inter-substituent CT. The former candidates are expected to significantly modify the electron distribution in the region of the catecholates. In view of the chelating ability of such a motif, one can also anticipate metal-to-ligand and ligand-to-metal charge transfer

[a] Dr. C. Aronica, A. Venancio-Marques, Dr. V. Robert, Prof. G. Lemerrier  
Université de Lyon, Laboratoire de Chimie, ENS-Lyon, CNRS  
46, Allée d'Italie, 69364 Lyon Cedex 07 (France)  
Fax: (+33)472728860  
E-mail: vincent.robert@ens-lyon.fr

[b] Dr. J. Chauvin  
Université Joseph Fourier, CNRS 5250, ICMG FR-2607  
Département de Chimie Moléculaire, B.P. 5  
38402 St Martin d'Hères (France)

[c] Prof. G. Lemerrier  
Université Reims Champagne-Ardenne, ICMR-UMR CNRS 6229  
Groupe Chimie de Coordination  
B.P. 1039, 51687 Reims Cedex 2 (France)  
Fax: (+33)326913243  
E-mail: gilles.lemerrier@univ-reims.fr

Supporting information for this article is available on the WWW under <http://dx.doi.org/10.1002/chem.200802325>.



Scheme 1. Synthesis and general atom numbering scheme, also used for NMR assignments (see Experimental Section), of catechol compounds **pCat-I-PENO<sub>2</sub>**, **pCat-I-PENMe<sub>2</sub>**, **pCat-PENO<sub>2</sub>-PENMe<sub>2</sub>**, **pCat-PENO<sub>2</sub>-PEOMe**, **pCat-di-PEOMe** and **pCat-di-PECF<sub>3</sub>**. TBDMS = *tert*-butyldimethylsilyl.

(MLCT and LMCT, respectively). This is to be contrasted with the use of a (D,A)-substituted ligand, which should favour ILCT (intra-ligand CT) over MLCT and LMCT. Therefore, the synthesis, characterisation and theoretical analysis of these target systems should provide new insights into the rational design of chromophores and NLO-phore ligand-type materials. In this study, the tuning of the optical properties of a novel class of 4,5-[(4-substituted-phenylethynyl)] TBDMS-protected catecholate molecules is reported. Substitution of an electron donor and/or acceptor group at the 4- and 5-position(s) gives rise to different CT strengths and pathways within the chromophore. A correlation between these optical properties and the structures is suggested and complementary theoretical investigations performed. Density functional theory has allowed the calculation of polarisabilities and offers a quantitative analysis of the substituent effects.

## Results and Discussion

**Synthesis:** Compounds **1–3** (see Scheme 1), **pCat-di-PENO<sub>2</sub>** and **pCat-di-PENMe<sub>2</sub>** (Z=NO<sub>2</sub> and NMe<sub>2</sub>, respectively, as shown in Scheme 1) were prepared according to procedures previously described in the literature (see the Experimental Section for references). 4,5-Disubstituted TBDMS-protected

catechols **pCat-I-PENO<sub>2</sub>**, **pCat-I-PENMe<sub>2</sub>**, **pCat-di-PEOMe** and **pCat-di-PECF<sub>3</sub>** were obtained by Sonogashira cross-coupling reactions<sup>[4]</sup> starting from **1** and **2** (1 equiv) or **3** (1 equiv) or **4** (2 equiv) and commercially available 1-ethynyl-4-trifluoromethylbenzene (**5**), respectively, and starting from compound **pCat-I-PENO<sub>2</sub>** and **3** (1 equiv) or **4** (1 equiv) to obtain compounds **pCat-PENO<sub>2</sub>-PENMe<sub>2</sub>** and **pCat-PENO<sub>2</sub>-PEOMe**, respectively (see Scheme 1).

The yields were quite poor for monosubstituted compounds **pCat-I-PENO<sub>2</sub>** and **pCat-I-PENMe<sub>2</sub>** (around 20%, also obtained with the disubstituted product) and ranged from 40 to 53% for the disubstituted compounds **pCat-PENO<sub>2</sub>-PENMe<sub>2</sub>**, **pCat-PENO<sub>2</sub>-PEOMe**, **pCat-di-PEOMe** and **pCat-di-PECF<sub>3</sub>** (see the Experimental Section).

The electronic absorption spectra of the compounds in CH<sub>2</sub>Cl<sub>2</sub> are shown in Figure 1.

Three types of bands are observed. 1) Bands at around 230 nm that depend slightly on the substituent. These can be mainly attributed to  $\pi-\pi^*$  electronic transitions centred on the aromatic ring. 2) Lower-energy absorption bands lying in the 280–420 nm spectral range (revealing a shoulder at a higher wavelength), which may be mainly assigned to a donor–acceptor CT. 3) A broad band between 420 and 500 nm (the longest-wavelength  $\lambda_{\max}$ ) ascribed to the lower-energy CT between the strongest donor (for example, NMe<sub>2</sub>) and the acceptor (NO<sub>2</sub>). The low  $\epsilon$  values are consistent with the less-effective non-linear-conjugated pathway followed in this CT, which confirms the influence of the nature of the substituents and their positions on the maximum absorption wavelengths and  $\epsilon$  values.

Interestingly, the **pCat-PENO<sub>2</sub>-PENMe<sub>2</sub>** absorption spectrum is clearly very close to the arithmetic sum of the UV/Vis absorption of compounds **pCat-I-PENO<sub>2</sub>** and **pCat-I-PENMe<sub>2</sub>**, except for the lowest-energy absorption band attributed to a so-called “bent-conjugated pathway”,<sup>[5]</sup> which also confirms that the energy of the CT optical band-gap is further minimised in donor/acceptor-substituted compounds.

The absorption observed at 290 nm for the dimethoxy-substituted compound (**pCat-di-PEOMe**) is red-shifted to 320 nm in the spectrum of the bis(dimethylamino) compound (**pCat-di-PENMe<sub>2</sub>**) with a more efficient donor group (see Figure 1a). The same red-shift is observed for **pCat-di-**

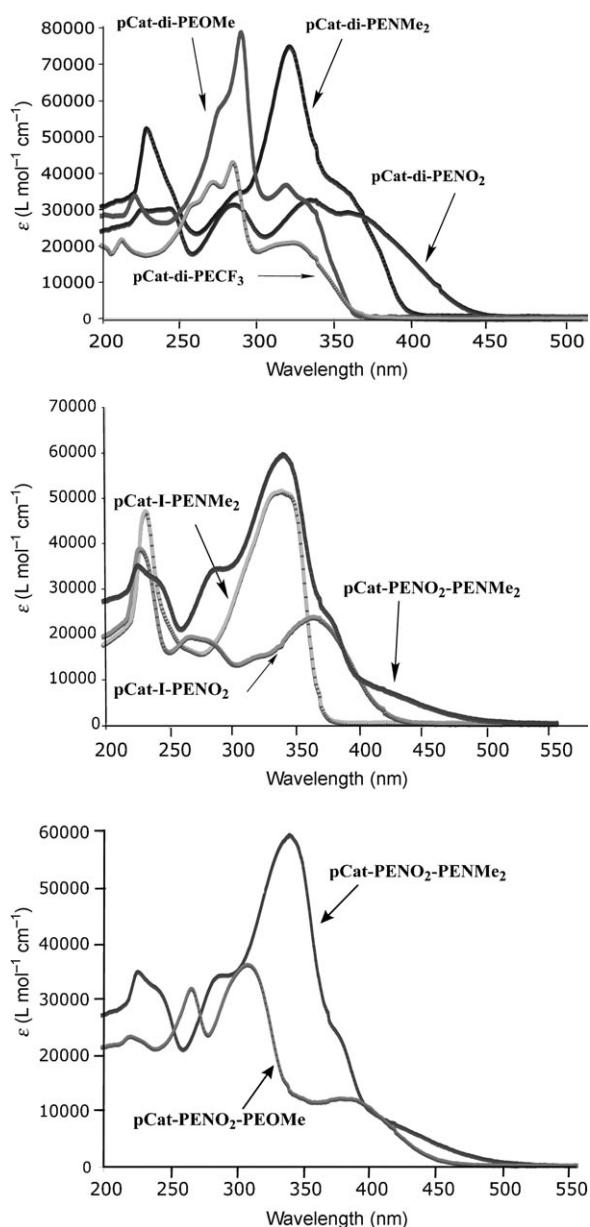


Figure 1. UV/Vis spectra of a) compounds **pCat-di-PEOMe**, **pCat-di-PENMe<sub>2</sub>**, **pCat-di-PENO<sub>2</sub>** and **pCat-di-PECF<sub>3</sub>**, b) compounds **pCat-I-PENMe<sub>2</sub>**, **pCat-I-PENO<sub>2</sub>** and **pCat-PENO<sub>2</sub>-PENMe<sub>2</sub>** and c) compounds **pCat-PENO<sub>2</sub>-PEOMe** and **pCat-PENO<sub>2</sub>-PENMe<sub>2</sub>** in dichloromethane.

**PECF<sub>3</sub>** and the dinitro analogue, which shows the intermediate character of the methoxy and trifluoromethyl substituents. It can also be seen in Figure 2 that this band is red-shifted as the polarity of the solvent is increased. The largest red-shift is observed for the dinitro compound **pCat-di-PENO<sub>2</sub>** due to the electron-donating character of the two OTBDMS groups in the *para* positions.

A systematic study of the linear optical properties of these compounds using different solvents has been accomplished. As an example, the results obtained for **pCat-di-**

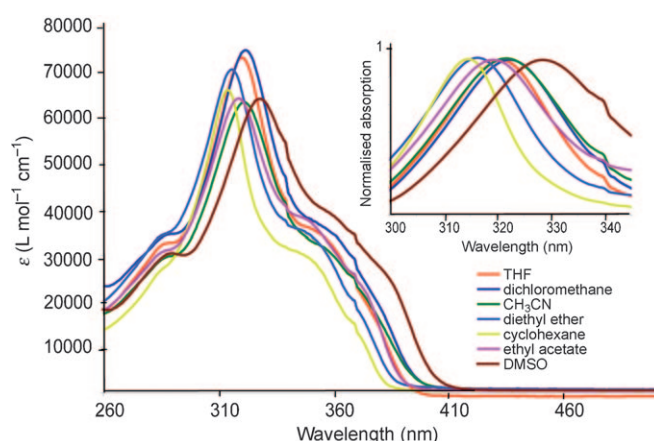


Figure 2. UV/Vis spectra of compounds **pCat-di-PENMe<sub>2</sub>** in several solvents (the insert represents a normalised section of the spectra).

**PENMe<sub>2</sub>** in relation to its absorption and emission properties are presented in Figures 2 and 4, respectively.

The CT bands display a positive solvatochromism, in good agreement with the increase in the dipole moment from the ground to the excited states (e.g.,  $\lambda_{\max}$  for **pCat-di-PENMe<sub>2</sub>**: cyclohexane, 315 nm; diethyl ether, 316 nm; ethyl acetate, 318 nm; THF, 320 nm; dichloromethane, 322 nm; CH<sub>3</sub>CN, 322 nm; DMSO, 328 nm). The UV/Vis spectra of molecules possessing only donor or acceptor functionalities usually lack CT transitions and display much reduced solvent dependencies.

**Fluorescence spectroscopy:** Several of the examined compounds showed fluorescence emission in solution at room temperature, as summarised in Table 1, but no (or very weak) emission was observed for the nitro-substituted compounds. The use of CF<sub>3</sub> is therefore interesting because it is the only acceptor group that allows experimental analysis of the luminescent properties. The luminescence spectra (displayed in Figure 3) exhibit broad bands centred at 370, 390 and 415 nm for compounds **pCat-di-PEOMe**, **pCat-I-**

Table 1. Absorption and emission properties of all the studied protected-compounds at room temperature and in the THF.

| Compounds                                      | $\lambda_{\text{abs}}$ [nm] ( $\epsilon$ [L mol <sup>-1</sup> cm <sup>-1</sup> ]) | $\lambda_{\text{em}}$ [nm] | Stokes shift [cm <sup>-1</sup> ] | $\phi$ <sup>[a]</sup> | $\tau$ <sup>[a]</sup> [ns] |
|--|---|----------------------------|----------------------------------|-----------------------|----------------------------|
| <b>pCat-I-PENO<sub>2</sub></b>                 | 355 (24275)   | 420                        | 4359                             | < 10 <sup>-4</sup>    | 2.11                       |
| <b>pCat-I-PENMe<sub>2</sub></b>                | 337 (47100)   | 418                        | 5750                             | 0.001                 | 2.81                       |
| <b>pCat-PENO<sub>2</sub>-PENMe<sub>2</sub></b> | 338 (59560)   | 420                        | 5776                             | 0.003                 | 2.88                       |
| <b>pCat-PENO<sub>2</sub>-PEOMe</b>             | 307 (32200)   | 543                        | 8180                             | 2 × 10 <sup>-4</sup>  | 0.71                       |
| <b>pCat-di-PEOMe</b>                           | 290 (88000)   | 362                        | 3626                             | 0.15                  | 1.26                       |
| <b>pCat-di-PENO<sub>2</sub></b>                | 329 (35000)   | 500                        | 7778                             | 0.001                 | 0.59                       |
| <b>pCat-di-PENMe<sub>2</sub></b>               | 322 (72760)   | 415                        | 6960                             | 0.21                  | 2.63                       |
| <b>pCat-di-PECF<sub>3</sub></b>                | 321 (20200)   | 395                        | 5900                             | 0.14                  | 2.03                       |

[a] In acetonitrile.

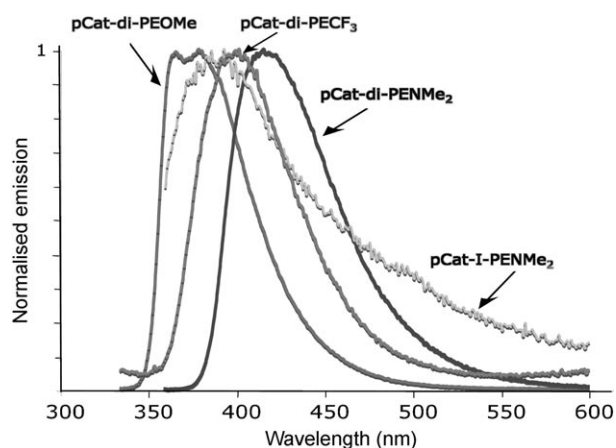


Figure 3. Normalised fluorescence emission of compounds **pCat-di-PEOMe**, **pCat-I-PENMe<sub>2</sub>**, **pCat-di-PECF<sub>3</sub>** and **pCat-di-PENMe<sub>2</sub>** in dichloromethane.

**PENMe<sub>2</sub>** and **pCat-di-PENMe<sub>2</sub>**, respectively. Maximum absorption and emission wavelengths, Stokes shifts ( $\Delta\nu_{ST}$ , defined as the loss of energy between the absorption and emission of light), quantum yields and excited-state lifetimes of all the compounds are reported in Table 1. A strong fluorescence has already been observed for a similar catechol substituted with two pyridine groups,<sup>[6]</sup> which was attributed to a  $\pi$ - $\pi^*$  transition. In our case, the dependence of the maximum emission wavelength on solvent polarity (see Figure 4

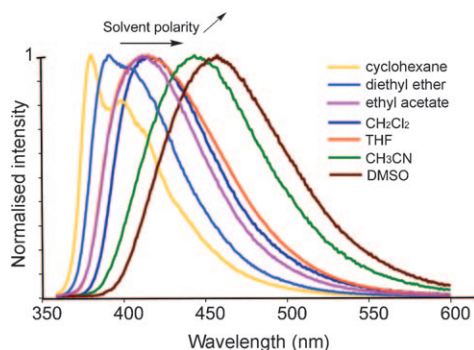


Figure 4. Emission spectra of compound **pCat-di-PENMe<sub>2</sub>** in different solvents.

for compound **pCat-di-PENMe<sub>2</sub>**) suggests that the fluorescence properties are instead due to a CT-type excited state.

The photophysical properties of **pCat-PENO<sub>2</sub>-PEOMe** and **pCat-di-PENO<sub>2</sub>** are markedly different from the other protected catecholates. The emission is dominated by a broad and red-shifted band with a larger Stokes shift, a lower quantum yield and a shorter emission lifetime.

These results suggest a larger rearrangement of the electronic distribution in the excited state of these structures prior to relaxation. For **pCat-PENO<sub>2</sub>-PEOMe**, this is in ac-

cordance with a large delocalisation of the electronic density from the PEOMe donor branch to the PENO<sub>2</sub> acceptor one.

The Stokes shift has been plotted against the solvent Reichardt  $E_T^N$  parameter<sup>[7]</sup> and its orientation polarisability  $\Delta f(\epsilon, n)$  (see Figure 5a and b, respectively; see also Table 2

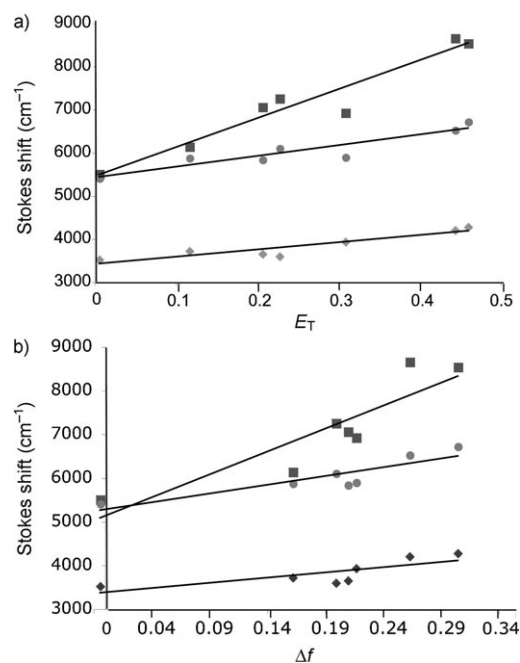


Figure 5. a) Plot of the Stokes shift ( $\Delta\nu_{ST}$ ) against the normalized Reichardt's  $E_T^N$  parameter. b) Correlation of the Stokes shift and the Lippert–Mataga polarity parameter according to Equation (1) for compounds **pCat-di-PENMe<sub>2</sub>** (■), **pCat-di-PEOMe** (◆) and **pCat-di-PECF<sub>3</sub>** (●) in the seven solvents listed in Table 2 ( $R^2=0.93, 0.87$  and  $0.85$  for compounds **pCat-di-PENMe<sub>2</sub>**, **pCat-di-PEOMe** and **pCat-di-PECF<sub>3</sub>**, respectively).

Table 2. Relative permittivity ( $\epsilon$ ) at 25 °C, refractive index ( $n$ ), orientational polarisability ( $\Delta f$ ) and Reichardt's  $E_T^N$  values of solvents.

| Solvents           | $\epsilon^{25^\circ\text{C}}$ | $n_D^{20}$ | $\Delta f(\epsilon, n)$ | $E_T^N$ |
|--------------------|-------------------------------|------------|-------------------------|---------|
| cyclohexane        | 2.0                           | 1.426      | -0.00396                | 0.006   |
| diethyl ether      | 4.2                           | 1.353      | 0.16223                 | 0.117   |
| ethyl acetate      | 6.0                           | 1.372      | 0.19943                 | 0.228   |
| THF                | 7.6                           | 1.407      | 0.20987                 | 0.207   |
| dichloromethane    | 8.9                           | 1.424      | 0.21692                 | 0.309   |
| CH <sub>3</sub> CN | 35.9                          | 1.344      | 0.30459                 | 0.460   |
| DMSO               | 46.4                          | 1.479      | 0.26308                 | 0.444   |

for further details). The relationship between the Stokes shift and the solvent polarity is usually given by the Lippert–Mataga equation [Eq. (1)].<sup>[8]</sup> This correlation is the equation most widely used to describe the effects of the physical properties of the solvent on the emission spectra of fluorophores. It has been used here to estimate the variation ( $\mu_{CT}-\mu_g$ ) in the dipole moment between the ground and the excited states (polarisability) with  $a$  representing the value of the Onsager cavity radius in which the fluorophore resides,<sup>[9]</sup>  $h$  is Planck's constant,  $c$  is the speed of light,  $\epsilon_0$  is the

vacuum permittivity and  $\Delta f(\epsilon, n)$  is defined by Equation (2) in which  $\epsilon$  is the static dielectric constant and  $n$  is the refractive index of the solvent.

$$\Delta\nu_{\text{ST}} = \Delta\nu_{\text{ST}}^0 + \left| \frac{2}{(4\pi\epsilon_0)(hca^3)} \right| \times (\mu_{\text{CT}} - \mu_{\text{g}})^2 \times \Delta f(\epsilon, n) \quad (1)$$

$$\Delta f(\epsilon, n) = \frac{\epsilon - 1}{2\epsilon + 1} - \frac{n^2 - 1}{2n^2 + 1} \quad (2)$$

The plots were linear for compounds **pCat-di-PENMe<sub>2</sub>**, **pCat-di-PEOMe** and **pCat-di-PECF<sub>3</sub>** with correlation factors of  $R^2 = 0.93$ ,  $0.87$  and  $0.85$ , respectively (for the plots against the  $E_{\text{T}}^{\text{N}}$  parameter), which suggests that dipole–dipole interactions between the solute and solvent are mainly responsible for the solvent-dependent fluorescence shift.

On the basis of Equation (1) and by assuming that the cavity radius  $a$  is comparable for compounds **pCat-di-PENMe<sub>2</sub>**, **pCat-di-PECF<sub>3</sub>** and **pCat-di-PEOMe**, the difference in the dipole moment between the ground and the excited states in solution is larger for the diamino compound than for the trifluoromethyl- and methoxy-substituted ones. With **pCat-di-PEOMe** as a reference (due to the homogeneous OR-type tetrasubstitution of the central aromatic ring), the slope, which is proportional to  $(\mu_{\text{CT}} - \mu_{\text{g}})^2$  according to Equation (1), is 4.3- and 1.7-fold larger for **pCat-di-PENMe<sub>2</sub>** and **pCat-di-PECF<sub>3</sub>**, respectively. This indicates that the polarisability should be larger for **pCat-di-PENMe<sub>2</sub>** and that, as reported recently in the literature,<sup>[10]</sup> a higher efficiency in non-linear optics may be expected. The emission lifetime decay of the compounds in deoxygenated CH<sub>3</sub>CN, recorded at 480 nm after excitation at 400 nm, are all mono-exponential. The emission decay times  $\tau$  (see Table 1) of around a few nanoseconds are in good agreement with a singlet excited-state emission.

**X-ray structures:** Single crystals of deprotected **Cat-I-PENO<sub>2</sub>** and **Cat-di-PENO<sub>2</sub>** were obtained by slow evaporation of methanol and diethyl ether, respectively, after deprotection of the silyl groups in a tetrabutylammonium fluoride solution in THF.<sup>[11]</sup> On the molecular scale (Figure 6), **Cat-I-PENO<sub>2</sub>** is totally planar with all bonds having the expected bond lengths.

The dinitro compound **Cat-di-PENO<sub>2</sub>** exhibits a small dihedral C17–C5–C4–C9 angle (see Table 3) and the two nitrophenyl fragments are twisted from the catechol ring by 10°, thus the molecule exhibits an imperfect planarity. This particular geometry may be caused by steric interactions between the hydrogen atoms of each substituted aromatic cycle.

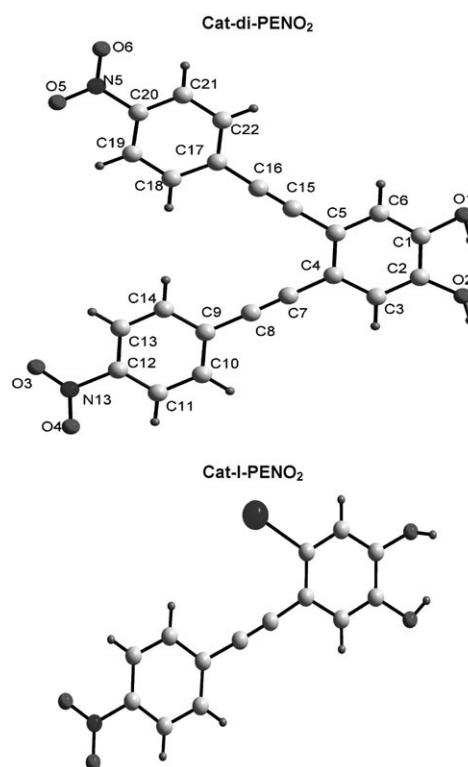


Figure 6. X-ray structures of **Cat-di-PENO<sub>2</sub>** and **Cat-I-PENO<sub>2</sub>** after deprotection (atom numbering for compound **Cat-di-PENO<sub>2</sub>** is used in Table 3).

**Theoretical analysis:** To support and rationalise our experimental data, complementary calculations based on DFT were performed. Our goal was to use a theoretical investigation to complement the experimental data obtained for **pCat-di-PENMe<sub>2</sub>**, **pCat-di-PEOMe** and **pCat-di-PECF<sub>3</sub>**. Although these compounds exhibit rather low polarisabilities, (see Figure 5b, the Lippert–Mataga plot), the **pCat-di-PENMe<sub>2</sub>** system looks like a promising candidate for non-linear optics applications.

In addition, the lack of experimental data on **pCat-di-PENO<sub>2</sub>** and **pCat-PENO<sub>2</sub>-PENMe<sub>2</sub>** (which do not exhibit any fluorescence under the experimental conditions used for this study) strongly supports the need for complementary theoretical inspections. How much the structures and combi-

Table 3. Geometric data extracted from X-ray analysis of **pCat-di-PENO<sub>2</sub>** and DFT-optimised parameters of **pCat-di-PENO<sub>2</sub>** and **pCat-di-PENMe<sub>2</sub>**. The relative orientations of the NO<sub>2</sub> groups and aryl rings are given.<sup>[a]</sup>

|                            | X-ray data | Optimised parameter             |                                  |
|----------------------------|------------|---------------------------------|----------------------------------|
|                            |            | <b>pCat-di-PENO<sub>2</sub></b> | <b>pCat-di-PENMe<sub>2</sub></b> |
| C17–C5–C4–C9               | 1.75       | 3.11                            | 3.39                             |
| (N13–O3–O4)/(C10–C12–C14)  | 8.00       | 0.34                            | 1.19                             |
| (N5–O5–O6)/(C18–C20–C22)   | 8.66       | 0.31                            | 1.16                             |
| (C9–C11–C13)/(C17–C19–C21) | 9.02       | 19.44                           | 21.56                            |
| (C9–C11–C13)/(C2–C4–C6)    | 10.48      | 15.61                           | 17.46                            |
| (C17–C19–C21)/(C1–C3–C5)   | 10.51      | 16.63                           | 17.48                            |
| C15–C16                    | 1.17       | 1.23                            | 1.23                             |
| C7–C8                      | 1.19       | 1.23                            | 1.23                             |

[a] All angles are in ° and distances in Å.

nations of donor and acceptor substituents compete in the generation of high polarisabilities might be scrutinised on the basis of ab initio calculations. First, a comparison was made between available experimental structures and calculated ones to validate the optimisation procedure. To reduce the computational cost, the OTBDMS groups were changed to methoxy groups; such a modification is unlikely to significantly modify the investigated properties (for convenience, the same “protected” term and “pCat” abbreviation will be used). Then we performed linear-response-type calculations to evaluate the polarisabilities. Finally, the impact upon the polarisabilities of the geometrical changes was estimated by allowing substituent changes without performing geometry optimisation.

The commonly accepted B3LYP (Becke–Lee–Yang–Parr) exchange-correlation functional was used throughout the geometry optimisations and linear-response-type polarisability calculations. Nevertheless, particular attention was paid to the dependence of the optical properties on the basis set used. In fact, it is known from the literature that sufficiently large basis sets are recommended to evaluate polarisabilities.<sup>[12]</sup> Such a procedure allows us to estimate the error bars in the polarisability calculations. Thus, we used the following strategy: First, full geometry optimisations of the disubstituted systems were carried out because the crystal structures were not available. These DFT calculations were conducted by using the B3LYP functional and the 6-311G basis set available in the Gaussian 03 package.<sup>[13]</sup> Such a combination of basis set and functional is known to produce very satisfactory optimised geometries for organic molecules. The calculated structure of **pCat-di-PENO<sub>2</sub>** is in good agreement with our X-ray data. In particular, this (A,A) compound exhibits a dihedral angle close to 3°, as expected from experimental diffraction data (1.8°). Therefore, a similar procedure was used for the whole series of compounds. The structural data for **pCat-di-PENO<sub>2</sub>** and **pCat-di-PENMe<sub>2</sub>** are reported in Table 3.

Let us first concentrate on the polarisabilities calculated for the protected **pCat-di-PENO<sub>2</sub>**, **pCat-di-PECF<sub>3</sub>**, **pCat-di-PEOMe** and **pCat-di-PENMe<sub>2</sub>** species by using the 6-311G basis set. CF<sub>3</sub> and MeO are known to be weak acceptor and donor substituents, respectively. Therefore, the corresponding systems display the lowest polarisabilities (≈360 and 370 Bohr<sup>3</sup>, respectively) in the series. The significant enhancement observed for the **pCat-di-PENMe<sub>2</sub>** compound (410 Bohr<sup>3</sup>) is in good agreement with the increase in the slope observed in Figure 5. As expected, the stronger donor character of the NMe<sub>2</sub> group relative to the methoxy group leads to a significant change in the polarisability. Even though experimental data for the **pCat-di-PENO<sub>2</sub>** molecule were not accessible, our calculations suggest that its polarisability should be comparable (see Figure 7a). One may therefore wonder why the (A,A) and (D,D) combinations represented by the **pCat-di-PENO<sub>2</sub>** and **pCat-di-PENMe<sub>2</sub>** synthetic compounds induce similar polarisability values. Part of the answer is to be found in the geometrical changes that accompany the changes of the substituents. Thus, bear-

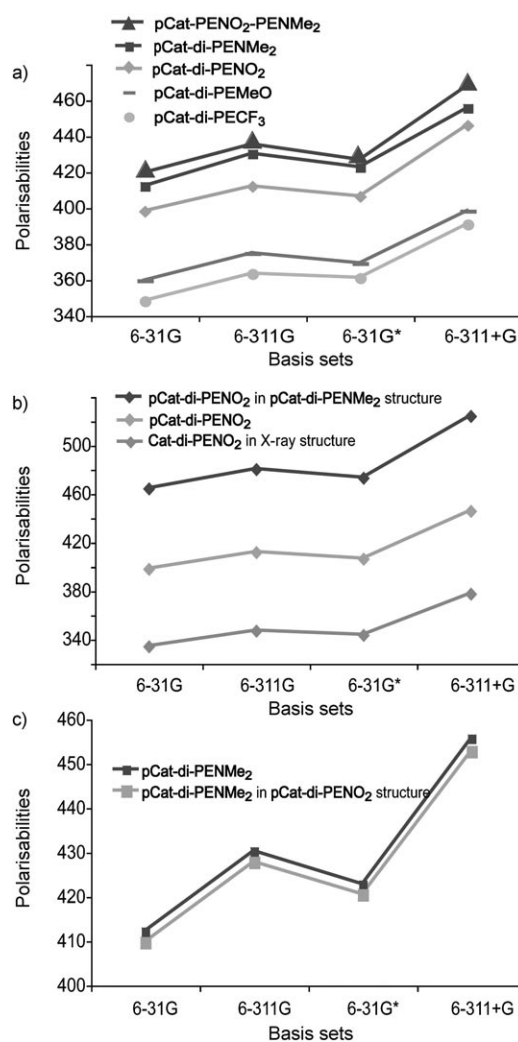


Figure 7. Theoretical values of the polarisabilities (in Bohr<sup>3</sup>) determined by different quality basis sets.

ing in mind that we are seeking to design molecules through a chemical engineering approach, we investigated this particular issue by using the X-ray and geometry-optimised structures obtained.

Based on these optimised geometries, polarisabilities were also calculated by using different basis sets and the molecular orbitals (MOs) were analysed to clarify the origins of the variations of the optical properties. The DFT-based polarisabilities are shown in Figure 7a as a function of basis-set quality. Even though it is traditionally accepted that 6-31G\* gives satisfactory estimates, we felt that a detailed inspection of the basis-set dependence for this class of compounds would be useful. As seen in Figure 7a, the variations in the polarisabilities with the different basis sets are very similar for the target molecules.

Not only do the parallel variations suggest that DFT calculations anticipate the relative polarisabilities, but one can also estimate the errors inherent in the numerical simulations. Hence, a 12% variation is observed as the basis set is modified. Let us stress that the calculations performed with

more elaborate basis sets than 6-311+G remained out of reach due to the relatively large size of the studied systems.

From this preliminary inspection, **pCat-di-PENO<sub>2</sub>** and particularly **pCat-di-PENMe<sub>2</sub>** and **pCat-PENO<sub>2</sub>-PENMe<sub>2</sub>** are observed to exhibit comparable polarisabilities ( $\approx 400$  Bohr<sup>3</sup>). These values were calculated by using the corresponding DFT-optimised structures. Thus, one may wonder how sensitive the polarisability is to geometrical changes. Because X-ray diffraction data are available for **Cat-di-PENO<sub>2</sub>**, a comparison between the polarisabilities obtained from 1) the X-ray data, 2) DFT-optimised data and 3) the optimised **pCat-di-PENMe<sub>2</sub>** structure was performed (see Figure 7b; the third value was determined by using the optimised structure of **pCat-di-PENMe<sub>2</sub>** to evaluate the influence of the geometrical changes ascribed to the substituents). A similar analysis was carried out for **pCat-di-PENMe<sub>2</sub>** for which X-ray data are not accessible (see Figure 7c). As seen in Figure 7b, the polarisability values are very sensitive to geometrical changes. The X-ray and optimised structures are very similar, but the corresponding polarisabilities differ by  $\approx 60$  Bohr<sup>3</sup>. A comparable difference is noted for calculations performed by using the **pCat-di-PENMe<sub>2</sub>** optimised structure. This is clear evidence of the important geometry dependency of the optical properties of **pCat-di-PENO<sub>2</sub>**. This is to be contrasted with the behaviour observed for **pCat-di-PENMe<sub>2</sub>** (Figure 7c). Whatever the geometry (i.e., optimised **pCat-di-PENMe<sub>2</sub>** or **pCat-di-PENO<sub>2</sub>**), the polarisability of **pCat-di-PENMe<sub>2</sub>** is in the 430 Bohr<sup>3</sup> range. One may argue that the acceptor character of the NO<sub>2</sub> substituent enhances CT within the molecule because the OMe group (OTBDMS analogue in the theoretical study) has a donor character. In turn, geometrical changes are likely to modify the polarisability. In particular, for complexes involving the **pCat-di-PENO<sub>2</sub>** deprotected analogue as a ligand (**Cat-di-PENO<sub>2</sub>**), significant variations can be anticipated. Conversely, the behaviour of the **pCat-di-PENMe<sub>2</sub>** molecule is different because the donor substituents NMe<sub>2</sub> and the OTBDMS analogue compete and reduce the sensitivity of the polarisability to geometrical modifications.

Finally, the valence molecular orbitals HOMO and LUMO were drawn to support the donor versus acceptor characteristics of the substituents. As shown in Figure 8, the LUMO has a strong NO<sub>2</sub> moiety character in **pCat-di-PENO<sub>2</sub>** and **pCat-PENO<sub>2</sub>-PENMe<sub>2</sub>**. The electron flow should be oriented towards NO<sub>2</sub> (see the arrows in Figure 8), in agreement with the substituent properties. As expected, the NMe<sub>2</sub> group exhibits donor characteristics because the HOMO in the **pCat-PENO<sub>2</sub>-PENMe<sub>2</sub>** compound is mostly localised on the NMe<sub>2</sub> moiety and the intramolecular CT to the LUMO can be selectively controlled. Note that the MeO substituent (introduced into the calculations to replace the OTBDMS moiety) does not seem to be involved in the CT in the **pCat-PENO<sub>2</sub>-PENMe<sub>2</sub>** analogue compound. As recently reported in the literature for dialkylamino- and/or pyridine-containing functional chromophores<sup>[14]</sup> and tetrakis(phenylethynyl)- or bis(dehydroben-

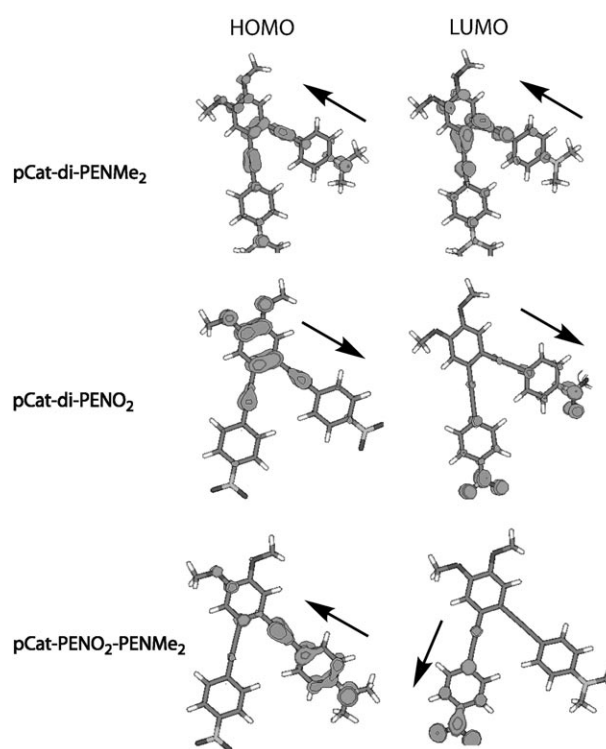


Figure 8. HOMO and LUMO valence MO diagrams for compound **pCat-di-PENMe<sub>2</sub>**, **pCat-di-PENO<sub>2</sub>** and **pCat-PENO<sub>2</sub>-PENMe<sub>2</sub>**.

zoannuleno)benzenes,<sup>[5]</sup> the donor and acceptor substituents tend to localise the disjoint frontier molecular orbitals (FMOs) on the corresponding branches of the so-called “cruciform”-type chromophores. Such compounds are known to exhibit remarkable optical properties, which have been studied, for instance, in diarylpyrazoline derivatives and exploited as biological sensory frameworks.<sup>[15]</sup> Because our compounds possess a “hemi-cruciform”-type structure, the presented catechol-derivatives provide an insight into CT behaviour.

## Conclusions

The synthesis and optical characteristics of NLO target molecules have been presented by following a chemical engineering approach. As far as molecular polarisability is concerned, it has been shown that their optical properties can be fine-tuned by an optical property–structure correlation. A low efficiency, red-shifted CT through a bent-conjugated pathway has been identified and compared with a more efficient linear-conjugated pathway. A theoretical study has also been performed and the results compared favourably with the experimental data. A systematic basis-set polarisability dependency was explored to validate the use of DFT/B3LYP calculations as theoretical probes. These calculations shed light on the crucial roles of structural and substituent effects. Related polarisability values and NLO properties were estimated. After the removal of the silyl-protecting

groups, the use of these molecules as ligands within complexes is under investigation and should lead to multifunctional coordination complexes, merging magnetic and optical properties. Because these substituted catecholate dianions are good metal-binding candidates, this preliminary study opens up new routes to multifunctional coordination complexes involving non-innocent ligands.<sup>[16]</sup>

## Experimental Section

**General:** All operations were performed under argon by using standard Schlenk-line techniques. All reagents and **4** were purchased from commercial sources and used as received. Compounds **1**,<sup>[17]</sup> **2**,<sup>[18]</sup> **3**,<sup>[18]</sup> **pCat-di-PENO<sub>2</sub>** and **pCat-di-PENMe<sub>2</sub>**<sup>[19]</sup> were prepared according to literature procedures.

**Instrumental:** <sup>1</sup>H and <sup>13</sup>C NMR spectra were recorded with a Bruker AC 200 FT NMR spectrometer. Elemental analyses were obtained from the "Service Central d'Analyse de Vernaison—CNRS". Infrared spectra were recorded in the range of 4000–200 cm<sup>-1</sup> as KBr pellets with a Mattson 3000 spectrometer. UV/Vis spectra were recorded with a Jasco V-550 spectrophotometer using spectro grade solvents. The steady-state emission spectra were recorded with a Photon Technology International (PTI) SE-900M spectrofluorimeter. All samples were prepared in a glove box in deoxygenated CH<sub>2</sub>Cl<sub>2</sub> and contained in 1 cm quartz cell. The samples were maintained in aerobic conditions with a Teflon cap. Emission quantum yields  $\phi_L$  were determined in deoxygenated CH<sub>3</sub>CN at 25 °C after irradiation at 360 nm (except for **pCat-PENO<sub>2</sub>-PEOME** for which an excitation wavelength of 340 nm was used) and by using a solution of anthracene in EtOH ( $\phi_L^{\text{Ref}} = 0.27^{[20]}$ ) as a standard according to Equation (3) in which  $I_L$ , the emission intensity, was calculated from the spectrum area  $\int I(\lambda) d\lambda$ ,  $OD$  represents the optical density at the excitation wavelength, the superscripts "S" and "Ref" refer to the sample and the standard, respectively, and  $n$  is the refractive index of the solvents. The time-dependant emission experiments were performed after irradiation at  $\lambda = 400$  nm obtained by the second harmonic of a titanium:sapphire laser (picosecond Tsunami laser spectra physics 3950-M1BB) at a 8 MHz repetition rate. Fluotime 200 from AMS technologies was used for decay acquisition. It consists of a GaAs microchannel plate photomultiplier tube (Hamamatsu model R3809U-50) and a time-correlated single-photon counting system from picoquant (PicoHarp300). The ultimate time resolution of the system was close to 40 ps. These measurements were recorded using the technical support from the chemistry platform "NanoBio Campus" in Grenoble (France).

$$\phi_L^S = \frac{I_L^S(1 - 10^{-OD^{\text{Ref}}})}{I_L^{\text{Ref}}(1 - 10^{-OD^S})} \frac{n_S^2}{n_{\text{Ref}}^2} \phi_L^{\text{Ref}} \quad (3)$$

**Typical general synthetic procedure for compounds Cat-I-PEX (X = NO<sub>2</sub>, NMe<sub>2</sub>), Cat-PENO<sub>2</sub>-PEY (Y = NMe<sub>2</sub>, OMe) and Cat-di-PEY (Y = OMe, CF<sub>3</sub>):** Compound **2** (0.5 g, 3.40 mmol) was added to a mixture of **1** (2 g, 3.39 mmol), [PdCl<sub>2</sub>(PPh<sub>3</sub>)<sub>2</sub>] (0.12 g, 0.17 mmol) and CuI (0.08 g, 0.42 mmol) in THF (100 mL) and Et<sub>3</sub>N (50 mL). The black solution was heated at 40 °C for 1.5 h (2 h for **Cat-di-PECF<sub>3</sub>**), cooled to room temperature and the solvent was evaporated under vacuum. The remaining black solid was purified by chromatography on silica gel (dichloromethane/petroleum ether, 2:3—except for **Cat-I-PENO<sub>2</sub>**, 1:3).

**pCat-I-PENO<sub>2</sub>:** Obtained as a pale-yellow solid (400 mg, 20% yield). <sup>1</sup>H NMR (200 MHz, CDCl<sub>3</sub>, 300 K):  $\delta = 8.20$  (AA', 2H), 7.69 (BB', 2H), 7.25 (s, 1H), 6.99 (s, 1H), 0.98 (s, 18H), 0.22 ppm (s, 12H); <sup>13</sup>C NMR (50 MHz, CDCl<sub>3</sub>, 300 K):  $\delta = 149.3$ , 147.3, 147.0, 132.1, 131.0, 130.3, 124.7, 123.7, 121.4, 97.0, 90.9, 89.4, 25.8, 18.5, -4.10 ppm; IR (KBr):  $\tilde{\nu} = 3112$  (vw, aryl C–H), 2956 (w, C–H), 2929 (w, C–H), 2885 (w, C–H), 2858 (w, C–H), 2208 (vw, C≡C), 1593 (w), 1577 (w), 1537 (w), 1514 (s, NO<sub>2</sub>), 1494 (w), 1479 (w), 1386 (vw), 1340 (s, NO<sub>2</sub>), 1324 (w), 1257 (vw), 1332 (vw), 1105 (vw), 998 (vw), 916 (w), 885(m), 864 (m), 849 (m), 785 (w), 750

(vw), 685 cm<sup>-1</sup> (m); UV/Vis (THF):  $\lambda_{\text{max}}$  ( $\epsilon$ ) = 355 nm (24275 mol<sup>-1</sup> dm<sup>3</sup> cm<sup>-1</sup>); HRMS:  $m/z$  calcd for C<sub>26</sub>H<sub>36</sub>Si<sub>2</sub>O<sub>4</sub>IN + Na<sup>+</sup>: 632.1125; found: 632.1120; elemental analysis calcd (%) for C<sub>26</sub>H<sub>36</sub>Si<sub>2</sub>O<sub>4</sub>I<sub>1</sub>N<sub>1</sub> (609.64): C 51.22, H 5.95, N 2.30; found: C 51.30, H 5.94, N 2.18.

**pCat-I-PENMe<sub>2</sub>:** Compound **1** (1.70 mmol), [PdCl<sub>2</sub>(PPh<sub>3</sub>)<sub>2</sub>] (0.08 mmol), CuI (0.21 mmol) in THF (20 mL), Et<sub>3</sub>N (10 mL) and **3** (1.70 mmol) gave 180 mg of a pale-yellow solid (18% yield); <sup>1</sup>H NMR (200 MHz, CDCl<sub>3</sub>, 300 K):  $\delta = 7.46$  (AA', 2H), 7.27 (s, 1H), 6.98 (s, 1H), 6.86 (BB', 2H), 2.98 (s, 6H), 0.99 (s, 18H), 0.22 ppm (s, 12H); <sup>13</sup>C NMR (50 MHz, CDCl<sub>3</sub>, 300 K):  $\delta = 150.2$ , 147.7, 147.1, 132.7, 130.8, 124.0, 123.6, 111.9, 110.0, 92.7, 90.5, 89.7, 40.3, 25.9, 18.5, -4.10 ppm; IR (KBr):  $\tilde{\nu} = 3093$  (vw, aryl C–H), 2954 (w, C–H), 2929 (w, C–H), 2893 (w, C–H), 2858 (w, C–H), 2206 (vw, C≡C), 1608 (w), 1579 (w), 1523 (w), 1481 (s), 1383 (w), 1360 (w), 1321 (vw), 1257 (s), 1190 (w), 1128 (vw), 995 (vw), 906 (vw), 881 (vw), 854 (w), 839(m), 814 (m), 783 (m), 712 (w), 532 (vw), 363 cm<sup>-1</sup> (m); UV/Vis (THF):  $\lambda_{\text{max}}$  ( $\epsilon$ ) = 337 nm (47100 mol<sup>-1</sup> dm<sup>3</sup> cm<sup>-1</sup>); HRMS:  $m/z$  calcd for C<sub>28</sub>H<sub>43</sub>Si<sub>2</sub>O<sub>2</sub>I<sub>1</sub>N<sub>1</sub> + H<sup>+</sup>: 608.1877; found: 608.1862; elemental analysis calcd (%) for C<sub>28</sub>H<sub>42</sub>Si<sub>2</sub>O<sub>2</sub>IN-0.2CH<sub>2</sub>Cl<sub>2</sub> (624.71): C 54.23, H 6.84, N 2.24; found: C 54.44, H 6.93, N 2.11.

**pCat-PENO<sub>2</sub>-PENMe<sub>2</sub>:** A mixture of **pCat-I-PENO<sub>2</sub>** (0.30 mmol), [PdCl<sub>2</sub>(PPh<sub>3</sub>)<sub>2</sub>] (0.01 mmol) and CuI (0.02 mmol) in THF (10 mL) with Et<sub>3</sub>N (5 mL) and **3** (0.43 mmol) yielded a pale-yellow solid (95 mg, 51% yield); <sup>1</sup>H NMR (200 MHz, CDCl<sub>3</sub>, 300 K):  $\delta = 8.17$  (AA', 2H), 7.64 (BB', 2H), 7.40 (AA', 2H), 6.98 (s, 2H), 6.64 (BB', 2H), 2.99 (s, 6H), 0.99 (s, 18H), 0.22 ppm (s, 12H); <sup>13</sup>C NMR (50 MHz, CDCl<sub>3</sub>, 300 K):  $\delta = 150.2$ , 148.6, 147.0, 146.7, 133.7, 132.6, 132.1, 130.9, 124.1, 123.8, 121.2, 117.5, 111.9, 110.0, 94.6, 94.0, 90.1, 85.8, 40.2, 25.9, 18.5, -4.10 ppm; IR (KBr):  $\tilde{\nu} = 3102$  (vw, aryl C–H), 2953 (w, C–H), 2926 (w, C–H), 2885 (w, C–H), 2856 (w, C–H), 2205 (vw, C≡C), 1608 (w), 1588 (w), 1527 (s, NO<sub>2</sub>), 1356 (w), 1337 (s, NO<sub>2</sub>), 1251 (s), 1191 (w), 1133 (vw), 1080 (vw), 923 (vw), 838 (vw), 779 (w), 685 cm<sup>-1</sup> (m); UV/Vis (THF):  $\lambda_{\text{max}}$  ( $\epsilon$ ) = 338 nm (59560 mol<sup>-1</sup> dm<sup>3</sup> cm<sup>-1</sup>); HRMS:  $m/z$  calcd for C<sub>36</sub>H<sub>46</sub>Si<sub>2</sub>O<sub>4</sub>N<sub>2</sub> + H<sup>+</sup>: 627.3074; found: 627.3071; elemental analysis calcd (%) for C<sub>36</sub>H<sub>46</sub>Si<sub>2</sub>O<sub>4</sub>N<sub>2</sub> (626.93): C 68.97, H 7.40, N 4.47; found: C 68.97, H 7.29, N 4.50.

**pCat-PENO<sub>2</sub>-PEOME:** A mixture of **pCat-I-PENO<sub>2</sub>** (0.30 mmol), [PdCl<sub>2</sub>(PPh<sub>3</sub>)<sub>2</sub>] (0.01 mmol) and CuI (0.02 mmol) in THF (10 mL), Et<sub>3</sub>N (5 mL) with **4** (0.43 mmol) yielded a pale-yellow solid (75 mg, 39% yield); <sup>1</sup>H NMR (200 MHz, CDCl<sub>3</sub>, 300 K):  $\delta = 8.17$  (AA', 2H), 7.63 (BB', 2H<sub>ar</sub>), 10-H), 7.46 (AA', 2H), 6.98 (s, 2H; 3-H, 6-H), 6.87 (BB', 2H), 2.99 (s, 3H), 0.99 (s, 18H), 0.22 ppm (s, 12H); <sup>13</sup>C NMR (50 MHz, CDCl<sub>3</sub>, 300 K):  $\delta = 159.8$ , 148.6, 147.4, 146.8, 132.9, 132.0, 130.7, 124.1, 124.0, 123.7, 120.5, 117.8, 115.4, 114.1, 113.7, 94.2, 92.6, 91.4, 86.5, 55.4, 25.9, 18.5, -4.01 ppm; IR (KBr):  $\tilde{\nu} = 3116$  (vw, aryl C–H), 2954 (w, C–H), 2927 (w, C–H), 2895 (w, C–H), 2856 (w, C–H), 2208 (vw, C≡C), 1590 (w), 1513 (s, NO<sub>2</sub>), 1406 (w), 1340 (s, NO<sub>2</sub>), 1247 (s), 1172 (w), 1083 (vw), 1028 (vw), 926 (vw), 837 (vw), 785 (w), 684 cm<sup>-1</sup> (m); UV/Vis (THF):  $\lambda_{\text{max}}$  ( $\epsilon$ ) = 307 (32200), 376 nm (10360 mol<sup>-1</sup> dm<sup>3</sup> cm<sup>-1</sup>); HRMS:  $m/z$  calcd for C<sub>35</sub>H<sub>43</sub>Si<sub>2</sub>O<sub>5</sub>N + Na<sup>+</sup>: 636.2578; found: 636.2556; elemental analysis calcd (%) for C<sub>35</sub>H<sub>43</sub>Si<sub>2</sub>O<sub>5</sub>N (613.89): C 68.48, H 7.06, N 2.28; found: C 68.47, H 7.07, N 2.06.

**pCat-di-PEOME:** A mixture of **1** (1 mmol), [PdCl<sub>2</sub>(PPh<sub>3</sub>)<sub>2</sub>] (0.14 mmol) and CuI (0.32 mmol) in THF (15 mL) with Et<sub>3</sub>N (7.5 mL) and **4** (2.2 mmol) yielded a pale-yellow solid (382 mg, 46% yield); <sup>1</sup>H NMR (200 MHz, CDCl<sub>3</sub>, 300 K):  $\delta = 7.47$  (AA', 2H), 6.96 (s, 2H), 6.84 (BB', 2H), 3.81 (s, 6H), 0.98 (s, 18H), 0.22 ppm (s, 12H); <sup>13</sup>C NMR (50 MHz, CDCl<sub>3</sub>, 300 K):  $\delta = 159.5$ , 147.3, 134.0, 133.6, 123.8, 119.6, 114.0, 91.9, 87.1, 55.3, 25.9, 18.5, -4.10 ppm; IR (KBr):  $\tilde{\nu} = 3005$  (vw, aryl C–H), 2952 (w, C–H), 2929 (w, C–H), 2896 (w, C–H), 2858 (w, C–H), 2208 (vw, C≡C), 1604 (w), 1515 (s, NO<sub>2</sub>), 1493 (w), 1353 (w), 1294 (vw), 1254 (s, NO<sub>2</sub>), 1171 (w), 1030 (vw), 931 (vw), 842 (vw), 825 (vw), 785 cm<sup>-1</sup> (w); UV/Vis (THF):  $\lambda_{\text{max}}$  ( $\epsilon$ ) = 290 nm (88000), 320 (42500 mol<sup>-1</sup> dm<sup>3</sup> cm<sup>-1</sup>); HRMS:  $m/z$  calcd for C<sub>36</sub>H<sub>46</sub>Si<sub>2</sub>O<sub>4</sub> + Na<sup>+</sup>: 621.2832; found: 621.283; elemental analysis calcd for C<sub>36</sub>H<sub>46</sub>Si<sub>2</sub>O<sub>4</sub> (598.9): C 72.19, H 7.74; found: C 72.26, H 7.46.

**pCat-di-PECF<sub>3</sub>:** A mixture of **1** (2.9 mmol), [PdCl<sub>2</sub>(PPh<sub>3</sub>)<sub>2</sub>] (0.57 mmol) and CuI (1.05 mmol) in THF (70 mL) with Et<sub>3</sub>N (35 mL) and **5**

(6.1 mmol) yielded a pale-yellow solid (1.02 g, 53% yield);  $^1\text{H NMR}$  (200 MHz,  $\text{CDCl}_3$ , 300 K):  $\delta$  = 7.60 (s, 8H), 7.02 (s, 2H), 1.01 (s, 18H), 0.26 ppm (s, 12H);  $^{13}\text{C NMR}$  (50 MHz,  $\text{CDCl}_3$ , 300 K):  $\delta$  = 148.2, 131.6, 130.3, 126.6, 125.3, 125.2, 121.2, 118.9, 90.8, 90.5, 25.9, 18.5, -4.10 ppm; IR (KBr):  $\tilde{\nu}$  = 2214  $\text{cm}^{-1}$  (vw,  $\text{C}\equiv\text{C}$ ); UV/Vis (THF):  $\lambda_{\text{max}}$  ( $\epsilon$ ) = 321 nm (20200  $\text{mol}^{-1}\text{dm}^3\text{cm}^{-1}$ ); HRMS:  $m/z$  calcd for  $\text{C}_{36}\text{H}_{40}\text{Si}_2\text{O}_2\text{F}_6 + \text{Na}^+$ : 697.2369; found: 697.2368; elemental analysis calcd (%) for  $\text{C}_{36}\text{H}_{40}\text{Si}_2\text{O}_4$  (598.9): C 64.1, H 5.97; found: C 63.8, H 5.90.

## Acknowledgements

The authors thank the "Centre de Diffractométrie H. Longchambon" of the University of Lyon for use of its X-ray diffraction facilities.

- [1] a) J. H. Burroughes, D. D. C. Radley, A. R. Brown, R. N. Marks, K. Mackay, R. H. Friend, P. L. Burns, A. B. Holmes, *Nature* **1990**, *347*, 539–541; b) R. H. Friend, R. W. Gymer, A. B. Holmes, J. H. Burroughes, R. N. Marks, C. Taliani, D. D. C. Bradley, D. A. Dos Santos, J. L. Brédas, M. Lögdlund, W. R. Salaneck, *Nature* **1999**, *397*, 992–996; c) T.-C. Chao, Y.-T. Lin, C.-Y. Yang, T. Shi Hung, H.-C. Chou, C.-C. Wu, K.-T. Wong, *Adv. Mater.* **2005**, *17*, 992–996; d) S. W. Thomas III, G. D. Joly, T. M. Swager, *Chem. Rev.* **2007**, *107*, 1339–1386.
- [2] a) Special Issue: *Chem. Rev.* **1994**, *94*, 1–278; b) J. Cornil, D. Beljonne, J.-P. Calbert, J.-L. Brédas, *Adv. Mater.* **2001**, *13*, 1053–1067; c) Special Issue: *Chem. Mater.* **2004**, *16*, 4381–4846.
- [3] a) R. R. Tykwinski, M. Schreiber, V. Gramlich, P. Seiler, F. Diederich, *Adv. Mater.* **1996**, *8*, 226–231; b) C. Bosshard, R. Spreiter, P. Günter, R. R. Tykwinski, M. Shreiber, F. Diederich, *Adv. Mater.* **1996**, *8*, 231–234.
- [4] K. Sonogashira in *Metal-Catalyzed Cross-Coupling Reactions* (Eds.: F. Diederich, P. J. Stang) Wiley-VCH, Weinheim, **1998**, pp. 203–230.
- [5] J. A. Marsden, J. J. Miller, L. D. Shirtcliff, M. M. Haley, *J. Am. Chem. Soc.* **2005**, *127*, 2464–2476.
- [6] a) S. Shotwell, P. Windscheif, M. Smith, U. Bunz, *Org. Lett.* **2004**, *6*, 4151–4154; b) M. G. Lauer, J. W. Leslie, A. Mynar, S. A. Stamper, A. D. Martinez, A. J. Bray, S. Negassi, K. McDonald, E. Ferraris, A. Muzny, S. McAvoy, C. P. Miller, K. A. Walters, K. C. Russell, *J. Org. Chem.* **2008**, *73*, 474–484.
- [7] C. Reichardt, *Chem. Rev.* **1994**, *94*, 2319–2358.
- [8] a) N. Mataga, *Bull. Chem. Soc. Jpn.* **1963**, *36*, 654–659; b) J. R. Lakowicz, *Principles of Fluorescence Spectroscopy*, Plenum Press, New York, **1983**.
- [9] The simplest method for estimating the cavity radius is to assume  $a = (3V/4\pi)^{1/3}$ , in which  $V$  is the volume of the solute.
- [10] F. Terenziani, C. Le Droumaguet, C. Katan, O. Mongin, M. Blanchard-Desce, *ChemPhysChem* **2007**, *8*, 723–734.
- [11] CCDC-706650 and 706651 contain the supplementary crystallographic data for this paper. These data can be obtained free of charge from the Cambridge Crystallographic Data Centre via [www.ccdc.cam.ac.uk/data\\_request/cif](http://www.ccdc.cam.ac.uk/data_request/cif).
- [12] P. J. P. de Oliveira, F. E. Jorge, *Chem. Phys. Lett.* **2008**, *463*, 235–239.
- [13] Gaussian 03, Revision C.02, M. J. Frisch, G. W. Trucks, H. B. Schlegel, G. E. Scuseria, M. A. Robb, J. R. Cheeseman, J. A. Montgomery, Jr., T. Vreven, K. N. Kudin, J. C. Burant, J. M. Millan, S. S. Iyengar, J. Tomasi, V. Barone, B. Mennucci, M. Cossi, G. Scalmani, N. Rega, G. A. Petersson, H. Nakatsuji, M. Hada, M. Ehara, K. Toyota, R. Fukuda, J. Hasegawa, M. Ishida, T. Nakajima, Y. Honda, O. Kitao, H. Nakai, M. Klene, X. Li, J. E. Knox, H. P. Hratchian, J. B. Cross, V. Bakken, C. Adano, J. Jaramillo, R. Gomperts, R. E. Stratmann, O. Yazyev, A. J. Austin, R. Cammi, C. Pomelli, J. W. Ochterski, P. Y. Ayala, K. Morokuma, G. A. Voth, P. Salvador, J. J. Dannenberg, V. G. Zakrzewski, S. Dapprich, A. D. Daniels, M. C. Strain, O. Farkas, D. K. Malick, A. D. Rabuck, K. Raghavachari, J. B. Foresman, J. V. Ortiz, Q. Cui, A. G. Baboul, S. Clifford, J. Cioslowski, B. B. Stefanov, G. Liu, A. Liashenko, P. Piskorz, I. Komaromi, R. L. Martin, D. J. Fox, T. Keith, M. A. Al-Laham, C. Y. Peng, A. Nanayakkara, M. Challacombe, P. M. W. Gill, B. Johnson, W. Chen, M. W. Wong, C. Gonzalez, J. A. Pople, Gaussian, Inc., Wallingford CT, **2004**.
- [14] A. J. Zuccherro, J. N. Wilson, U. H. F. Bunz, *J. Am. Chem. Soc.* **2006**, *128*, 11872–11881.
- [15] C. J. Fahmi, L. Yang, D. G. Vanderveer, *J. Am. Chem. Soc.* **2003**, *125*, 3799–3812.
- [16] E. Evangelio, D. Ruiz-Molina, *Eur. J. Inorg. Chem.* **2005**, 2957–2971.
- [17] J. D. Kinder, W. J. Youngs, *Organometallics* **1996**, *15*, 460–463.
- [18] S. Takahashi, Y. Kuroyama, K. Sonogashira, N. Hagihara, *Synthesis* **1980**, 628–630.
- [19] V. Kriegisch, C. Lambert, *Eur. J. Inorg. Chem.* **2005**, 4509–4515.
- [20] W. R. Dawson, M. W. Windsor, *J. Phys. Chem.* **1968**, *72*, 3251–3260.

Received: November 8, 2008  
Published online: March 31, 2009